HSR (LONDON),
HOUGHTON STREET REVIEW JOURNAL
ISSN: 2058-5519|Impact factor-15.9
http://houghtonstreetreview.com/index.php/hsr

UDK: 546.26.043:535

NANOAGGREGATION OF C_{60} FULLERENE IN A BENZENE/ISOPROPYL ALCOHOL BINARY SOLVENT SYSTEM: A COMPREHENSIVE ANALYSIS OF OPTICAL, REFRACTOMETRIC, RAMAN AND DYNAMIC LIGHT SCATTERING STUDIES

Sattarova Nilufar Abdulaziz qizi
Master's Student, National University of Uzbekistan named after Mirzo Ulugbek
Email: sattarovanilufar5@gmail.com

Doi: https://doi.org/10.5281/zenodo.23253612

Annotation. In this study, the process of forming nanoaggregates of C $_{60}$ fullerene molecules in a benzene and isopropyl alcohol (IPS)-based binary solvent system (IPS volume fraction 2–8%, C_{60} concentration 0.2 mg/ml) was investigated using a set of methods such as refractometry, areometry, UV–Vis optical absorption spectroscopy, dynamic light scattering (YDS), and Raman spectroscopy. With increasing IPS concentration, the refractive index of the solution decreased from 1.4949 to 1.4851, and the density decreased from 0.8672 to 0.8564 g/^{cm3}. According to the results of the YDS, the dominant cluster size in C $_{60}$/benzene solution was ≈17 nm, and when the IPS proportion was 2, 4, 6 and 8%, it increased to ≈20–40, ≈31, ≈80–120 and ≈150–220 nm, respectively, the system switched from monodisperse to polydisperse state. but rather a phased (monomer → solved state → clustering → large nanoaggregates) process, with the formation of a quasi-stable system at low IPS stakes (2–4%) and a destabilized system at high stakes (6–8%).

Keywords: C_{60} fullerene, benzene, isopropyl alcohol, nanoaggregation, self-organization, dynamic scattering of light, refractive index, density, Brix, Raman spectroscopy, UV–Vis.

Аннотация. В работе методами рефрактометрии, ареометрии, УФ–видимой спектроскопии поглощения, динамического рассеяния света (ДРС) и спектроскопии комбинационного рассеяния исследовано образование наноагрегатов молекул фуллерена C_{60} в бинарной системе растворителей бензол/изопропиловый спирт (ИПС) при объёмной доле ИПС 2–8 % и концентрации С60 0,2 мг/мл. С увеличением доли ИПС показатель преломления раствора уменьшается с 1,4949 до 1,4851, плотность — с 0,8672 до 0,8564 г/см3. По данным ДРС доминирующий размер кластеров в растворе С60/бензол составляет ≈17 нм и возрастает до ≈150–220 нм при 8 % ИПС; система переходит из практически монодисперсной в полидисперсную. Временная эволюция показателя преломления, плотности, значений Брикса и спектров КР в течение 1–12 суток показала ступенчатый характер агрегации: при 2–4 % ИПС формируются квазистабильные наноагрегаты, при 6–8 % наблюдаются дестабилизация системы и образование крупных агрегатов.

Ключевые слова: фуллерен С60, бензол, изопропиловый спирт, наноагрегация, самоорганизация, динамическое рассеяние света, показатель преломления, плотность, Брикс, спектроскопия КР.

HSR (LONDON),
HOUGHTON STREET REVIEW JOURNAL
ISSN: 2058-5519|Impact factor-15.9
http://houghtonstreetreview.com/index.php/hsr

Abstract. The formation of C60 fullerene nanoaggregates in a benzene/isopropyl alcohol (IPA) binary solvent system (IPA content 2–8 vol.%, C60 concentration 0.2 mg/ml) was studied by refractometry, areometry, UV–Vis absorption spectroscopy, dynamic light scattering (DLS) and Raman spectroscopy. With increasing IPA content, the refractive index decreased from 1.4949 to 1.4851 and the density from 0.8672 to 0.8564 g/cm^3. According to DLS, the dominant cluster size in C60/benzene is ≈17 nm and grows to ≈150–220 nm at 8 % IPA, the system turning from nearly monodisperse to polydisperse. Time-dependent measurements over 1–12 days revealed a stepwise aggregation pathway (monomer → solvated state → clustering → large nanoaggregates): quasi-stable aggregates form at 2–4 % IPA, whereas destabilization and large-aggregate formation occur at 6–8 % IPA.

Keywords: C60 fullerene, benzene, isopropyl alcohol, nanoaggregation, self-assembly, dynamic light scattering, refractive index, density, Brix, Raman spectroscopy.

1. INTRODUCTION

The Fullerene C60 molecule is one of the most studied nanoobjects due to its quasispheric structure, high icosahedric (Ih) symmetry, decalculated π-electron system, and high electron affinity [1]. Fullerene-based nanomaterials are used in nanoelectronics, optoelectronics, solar cells, electrochemical and optical sensors, biomedicine, and drug-transporting systems [2–4]. The properties of such materials are largely determined by the structural state of the fullerene solutions — whether the molecules exist individually or form clusters and nanoaggregates of different sizes.

C60 is good soluble in nonpolar aromatic solvents (benzene, toluene, xylene) and very poorly soluble in polar solvents (alcohols, water) [9, 10]. Therefore, the formation of fullerene colloidal particles and clusters is strongly manifested in binary systems consisting of good and bad solvents [5–8]. Since benzene is good for C 60 and isopropyl alcohol (IPS) is a bad solvent, the benzene–IPS system is a suitable model system for controlling the aggregation process through solvent composition and for controlled formation of nanoaggregates. The spontaneous organization of fullerene solutions has been shown to depend not only on concentration and type of solvent, but also on the method of preparation and storage time of the solution [11–14].

For qualitative evaluation of aggregation, UV–Vis and infrared spectroscopy, refractometry, and areometry are widely used, but the exact size and size distribution of aggregates can only be determined directly using the Dynamic Scattering of Light (YDS) method. In addition, in most studies, aggregation has been studied only in relation to solvent composition, and the effect of the time factor (aging effect) on structural evolution has not been adequately elucidated in combination with macroscopic physical parameters (refractive index, density, Brix) and microstructural method (Raman spectroscopy).

The purpose of this study is to determine the formation process of nanoaggregates in C 60/benzene/IPS solutions, their size and size distribution, and evolution over time on the basis of cross-comparison of the results of spectral (UV–Vis, Raman), optical-physical (refractive index, density, Brix) and YDS methods. To achieve the objective, the following tasks were set: (i) to determine the effect of IPS proportion (2–8%) on refractive index, density, and optical absorption; (ii) to measure the hydrodynamic size and distribution of aggregates using the YDS method; (iii) to study

HSR (LONDON),
HOUGHTON STREET REVIEW JOURNAL
ISSN: 2058-5519|Impact factor-15.9
http://houghtonstreetreview.com/index.php/hsr

the 1, 4, 8, and 12-day evolution of solutions; (iv) to propose an aggregation mechanism based on correlation between micro- and macroscopic parameters.

2. RESEARCH METHODOLOGY

2.1. Materials

In the experiments, C_{60} fullerene powder (purity >99.8%, Sigma-Aldrich), benzene (purity >99%) as a nonpolar solvent, and isopropyl alcohol (IPS, 99.7%) as the polar component were used. The diameter of the C 60 molecule $d_{is\,0} \approx 0.714$ nm, the refractive index $n \approx$ is 1.96, and the dielectric constant is $\varepsilon \approx 3.61$.

2.2. Preparation of samples

Initially, a basic solution of C 60/benzene was prepared: 8 mg of C_{60} powder was measured on an analytical scale and dissolved in 16 ml benzene at room temperature in an automated magnetic stirrer (2.0–2.2 Hz) for 45 min. The result was a homogeneous, molecular solution with a concentration of 0.5 mg/ml. Working C_{60}/benzene/IPS solutions were prepared from the same base solution, and the final concentration of C_{60} in all samples was kept at 0.2 mg/mL (total volume 5 mL: 2 mL main solution + benzene + IPS). The composition of the samples is shown in Table 1.

Table 1. Composition of C60/benzene/IPS solutions

IPS Share, %	Volumetric ratio benzene:IPS	Main solution (C_{60}/benzene), ml	Benzene, ml	IPS, ml
0	100:0	—	—	—
2	98:2	2	2,9	0,1
4	96:4	2	2,8	0,2
6	94:6	2	2,7	0,3
8	92:8	2	2,6	0,4

The prepared mixtures were dispersed in an ultrasonic bath (25 kHz) at a temperature of 10 °C for 20 min, followed by stabilization in a thermostat at 8 °C for 30–40 min. To study evolution over time, the samples were stored in hermetically sealed containers, protected from light, for 1, 4, 8, and 12 days, and remeasured at each stage.

2.3. Measurement methods

Optical absorption spectra were recorded on the UV–Vis 5100 spectrophotometer with a pitch of 0.5 nm in the range of 320–800 nm. Raman spectra were obtained using a Cobolt CW DPSS laser with

HSR (LONDON),
HOUGHTON STREET REVIEW JOURNAL
ISSN: 2058-5519|Impact factor-15.9
http://houghtonstreetreview.com/index.php/hsr

a wavelength of 532 nm as an excitatory source on the InVia Raman spectrometer (Renishaw, UK). The refractive index and Brix values were determined on the Atago PAL-BX/RI digital refractometer (measurement error ±0.0001; instrument based on Snellius' law; sample size ≤0.4 ml) per measurement. Density was measured on a METTLER TOLEDO DENSITO 30PX densitometer. Refractometric and densymmetric measurements were repeated three times and mean values were calculated; the temperature was kept under thermostatic control (≈24 ± 0.1 °C).

The particle size and size distribution of the disperse phase were determined using the YDS method in the Zetasizer Nano ZEN3600 system (Malvern Instruments Ltd., UK); the measurements for each solution were repeated three times. In the YDS method, fluctuations in the intensity of the scattered laser light due to the Brownian motion of the particles are analyzed; the hydrodynamic diameter d from the translational diffusion coefficient d is found by the Stokes–Einstein relationship:

$$dH = k_{IT} / (3\pi\eta D) \quad (1)$$

where k_B is the Bolsmann constant, T is the absolute temperature, η is the viscosity of the solvent. According to Maxwell's theory, the refractive index of the solution is related to the dielectric and magnetic properties of the medium as follows:

$$n2 = \varepsilon\mu / (\varepsilon_{0\mu 0}) \quad (2)$$

Where ε and ε_0 are the dielectric constants of the medium and vacuum, respectively, and μ and μ_0 are the magnetic resorptions.

3. RESULTS AND THEIR DISCUSSION

3.1. Dependence of Refractive Index and Density on IPS Proportion

As light passes through a fullerene solution, photons interact with the electric and magnetic fields generated by the molecules; this impact force determines the phase velocity of light, and therefore the refractive index. Density, on the other hand, reflects the degree of placement (packing) of molecules and can be one of the macroscopic indicators of spontaneous organization. Table 2 presents the measurement results for newly prepared solutions.

Table 2. Refractive index (n) and density (ρ) of C60/benzene/IPS solutions (at the time of preparation)

IPS Share, %	Refractive index, n	Density ρ, g/cm3
0	1,4949	0,8672
2	1,4923	0,8636
4	1,4906	0,8614
6	1,4904	0,8614
8	1,4851	0,8564

HSR (LONDON),
HOUGHTON STREET REVIEW JOURNAL
ISSN: 2058-5519|Impact factor-15.9
http://houghtonstreetreview.com/index.php/hsr

In pure C_{60}/benzene solution (0.5 mg/ml), the refractive index had the highest value (1.4949); as the IPS proportion increased, n gradually decreased, reaching a minimum value (1.4851) at 8% (Fig. 1, a). The density also showed a similar trend: 0.8672 g/^{cm3} decreased from 0.8564 g/cm3 to 0.8564 g/cm3 (Fig. 1, b). These changes reflect the redistribution of intermolecular interactions (fullerene–solvent and fullerene–fullerene) in solution with the addition of IPS and the change in the formation process of fullerene-specific nanostructures [14]. It should be noted that in solutions with 4 and 6 % IPS, the values of n and ρ are very close to each other (n: 1.4906 and 1.4904; ρ: 0.8614 and 0.8614), i.e. at this interval the solution parameters stabilize "plateau", while at 8% there is a more sharp decrease.

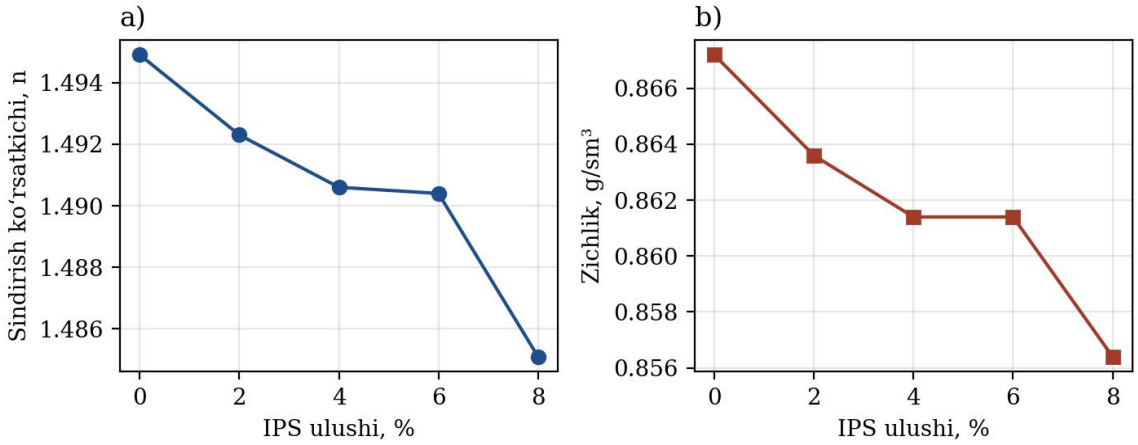


Figure 1. Correlation of refractive index (a) and density (b) to IPS volumetric proportion (based on data from Table 2)

3.2. Optical absorption spectra

In the absorption spectrum of the C60/benzene solution, fullerene-specific maximums were observed to be around 391, 407, 545, and 625 nm; they correspond to the π–π* electron transitions and vibronic structure of the C 60 molecule and are a spectral marker of the monomer state. The location of the maximums was virtually unchanged when IPS was added (407.2–407.7; 598.7; 625–626 nm), indicating that the C60 electron structure remained, but significant changes in intensity and baseline were observed. The loss of the monomer-specific 391 nm peak after the addition of IPS indicates that with increasing solvent polarity, π–π effects between C 60 molecules are enhanced and aggregation begins: the monomer-specific transitions expand and merge into a sphere around 407 nm [11, 13].

Although the concentration of C60 in all solutions was the same (0.2 mg/ml), the optical density was non-monotonous with the proportion of IPS. At an aggregation-sensitive peak of 598.7 nm, the optical density decreased to low values (≈0.1–0.25) at 2 and 4 % IPS, maximum (≈0.7) at 6 % IPS, and again lower at 8 % IPS. At 2–4 % IPS, the aggregation increases gradually; at 6%, the maximum optical density corresponds to the critical aggregation state, with the contribution of light scattering from the aggregates also contributing to absorption; The decrease in absorption at 8% is explained by

HSR (LONDON),
HOUGHTON STREET REVIEW JOURNAL
ISSN: 2058-5519|Impact factor-15.9
http://houghtonstreetreview.com/index.php/hsr

the formation of large clusters and their partial subsidence. The elevation of the baseline indicates an increase in light scattering. In both solutions (C60/benzene and C60/benzene/IPS), a deviation from the Buger–Lambert–Ber law was observed; this may be the result of a significant increase in fullerene–fullerene interactions and the formation of nanoaggregates. The observed hyperchromic and hypochromic effects are also associated with the variation of C60–C60 interactions under the influence of IPS molecules. This fact necessitates the direct measurement of aggregate size.

3.3. Dynamic light scattering: size and distribution of aggregates

In the images of the laser beam intensity fluctuations scattered in the YDS system, the tiny, independent particles give a uniform grain picture, while when aggregation occurs, the interference rings become larger, the central intensity increases, and the interference lines become more pronounced. For the C_{60}/benzene solution, many tiny, independent bright dots and soft, low-amplitude rings were observed in the image; this indicates that the fullerene in the solution is in a well-dissolved state, mainly in the form of individual molecules or small aggregates. In the C_{60}/benzene/IPS solution, on the other hand, the rings were much larger, the interference lines were denser, and a strong brightness was observed in the center, indicating that the particles were enlarged (aggregation increased). As a result of the addition of IPS, dipole-induction interactions on the fullerene surface are intensified, intermolecular gravity increases, Brownian motion slows down, and the average diameter measured in YDS increases; this result is consistent with the shift in the infrared spectra obtained earlier (535 → 517 cm^{-1}, softening of radial fashion).

In the C60/benzene solution (IPS = 0), the basic size maximums of the nanoclusters were observed to be around ≈17 nm; there are also small maximums around ≈55 and ≈135 nm in the distribution. This means that in benzene, fullerene is predominantly in the form of individual molecules or small clusters, and the 55 and 135 nm particles may be larger clusters formed by secondary aggregation. In the 4 % IPS solution, the distribution became much more complex, with several maximums (≈31, 60, 91, 128, and 200 nm); the highest concentration was for ≈31 nm particles. Thereby, the dominant cluster size increased from 17nm to 31nm when compared with a benzene solution, new aggregates appeared, in the range of 60–200nm, and the system moved from the monodisperse to the polydisperse state.

Table 3 summarizes the main features of the size distribution derived from the YDS histograms for solutions with IPS proportions of 2, 6, and 8%.

Table 3. Effect of IPS Fraction on Hydrodynamic Size Distribution of C_{60} Nanounits (YDS)

IPS, %	Basic maximum (dominant)	Other fractions	System status
0	≈17 nm	≈55 and ≈135 nm (small fraction)	Almost monodisperse; individual molecules/small clusters

HSR (LONDON),
HOUGHTON STREET REVIEW JOURNAL
ISSN: 2058-5519|Impact factor-15.9
http://houghtonstreetreview.com/index.php/hsr

IPS, %	Basic maximum (dominant)	Other fractions	System status
2	20–40 nm	50–80 nm; 100–150 nm (low); >200 nm is almost non-existent	Aggregation is in the initial stage; relatively low polydisperse
4	≈31 nm	≈60, 91, 128, 200 nm	polydisperse; increased clustering
6	80–120 nm	120–160 nm; 200–300 nm; 30–50 nm	Polydisperse; aggregation intensive
8	150–220 nm	300–400 nm; 500–650 nm; 20–50 nm fraction very low	Large aggregates dominant; close to coagulation stage

The YDS results clearly show that the level of aggregation is monotonous related to the share of IPS (Fig. 2): At IPS = 2%, aggregates predominate mainly in the range of 20–80 nm, in 6% 80–160 nm, and at 8%, aggregates of 150–400 nm and larger are formed. This is fully consistent with the fact that IPS is a poor solvent relative to fullerene and that the coalescence of fullerene molecules increases with an increase in its share.

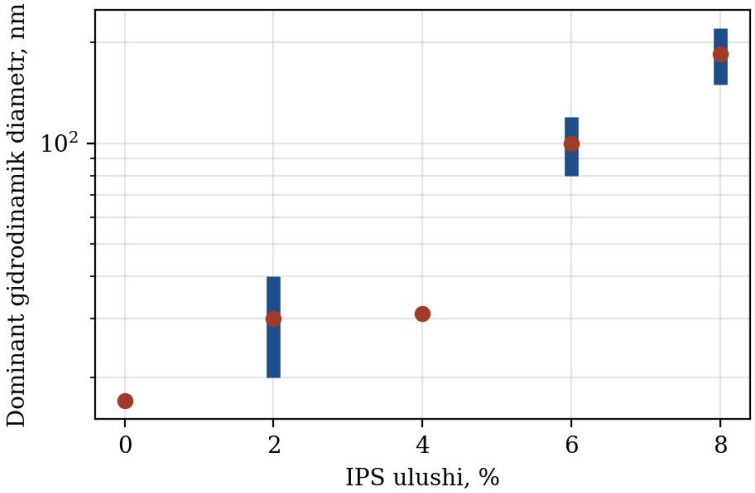


Figure 2. Dependence of the dominant hydrodynamic diameter on the share of IPS (YDS; vertical line is the dominant maximum range, point is the average value; IPS = the single maximum value for 0 and 4%)

HSR (LONDON),
HOUGHTON STREET REVIEW JOURNAL
ISSN: 2058-5519|Impact factor-15.9
http://houghtonstreetreview.com/index.php/hsr

3.4. Evolution of Refractive Point, Density, and Brix Values over Time

The evolution of the melts at 1, 4, 8, and 12 days was studied by fracture index, density, and Brix; the main results are summarized in Table 4.

Table 4. Change in C60/benzene/IPS solution parameters over 1–12 days (values are approximately derived from measurement graphs, denoted by "≈")

IPS, %	n(Day 1 → Day 12)	ρ, g/sm3 (day 1 → day 12)	Brix (Day 1 → Day 12)	General Trend
0	1.4947 → 1.491	≈0.867 → ≈0.863	82.6 → 81	Monotonous decline; clustering
2	≈1,492 → ≈1,493	≈0.864 → ≈0.863	≈81.7 → ≈81.7	Maximum in 4–8 days; Completion
4	≈1.4906 → ≈1.491	≈0.861 → ≈0.863	≈81.0 → ≈80.9	Maximum in 8 days; quasi-stable
6	≈1.4904 → ≈1.488	≈0.861 → ≈0.861	≈78.9 → ≈80.1	Sharp drop after 8 days
8	≈1.4851 → ≈1.483	≈0.856 → ≈0.856	≈81.4 → 78	The biggest decline; destabilization

Breaking Indicator. The decrease of n from 1.4947 to 1.491 in the C 60/benzene system indicates the transition of molecules over time from the individual disperse state to the clustered state: as a result of aggregation, the intermolecular distance is redistributed, the effective polarity of the medium and the optical density decreases. Stabilization of n by day 12 indicates that the system is approaching a quasi-equilibrium state. In systems with 6 and 8% IPS, n decreases sharply on day 12, which is explained by the formation of large nanoaggregates, increased polydispersity, and spatial heterogeneity of the system.

Brix. The value of brix represents the integral optical concentration of the solution and is sensitive to structural redistributions. The decrease in Brix in C 60/benzene solution from 82.6 to 81 indicates a violation of optical homogeneity as a result of aggregation. The increase in Brix in 2 and 4 % IPS at 4–8 days is explained by the compacting and reorganization of the clusters, the system transitions to a relatively stable nanoaggregate configuration. The sharp increase and subsequent decrease observed in 6 % IPS indicates the gradual kinetics of aggregation: first intensive clustering, followed by the formation of large aggregates. A decrease in Brix from 81.37 to 78 at 8 % IPS indicates a decrease in colloidal stability, the formation of large aggregates and partial sedimentation may occur.

HSR (LONDON),
HOUGHTON STREET REVIEW JOURNAL
ISSN: 2058-5519|Impact factor-15.9
http://houghtonstreetreview.com/index.php/hsr

Density. Density represents the degree of macroscopic structural organization of the system: the degree of spatial packaging increases as the intermolecular distance decreases. In the C_{60}/benzene system, the decrease in density in the early days indicates a transition to the clustering phase (the effective mass distribution decreases as there are empty spatial regions within the clusters). In 2–4 % IPS systems, the increase in density on days 4–8 is associated with the compacting and spatial density of the nanoaggregates; and in 6–8 % IPS solutions, the decrease in density by day 12 indicates spatial destabilization and an increase in macroscopic heterogeneity. The density results confirm the phase evolution of the C_{60} nanoaggregates, respectively, with the n and Brix phases.

3.5. Raman spectroscopy results

Raman spectra obtained on days 1 and 12 of C60/benzene and C60/benzene/IPS solutions (2–8%) made it possible to identify microstructural signs of aggregation. In all systems, the most intensive mode around ≈992–993 cm^{-1} was preserved. In the C_{60}/benzene spectrum on day 1, this peak is narrow, high-intensity and precisely localized, indicating that the molecules are predominantly disperse (monomer or small cluster) state, and microheterogenicity is minimal. By day 12, a decrease in peak contrast, line expansion and an increase in spectral background were observed: line expansion indicates a variety of local media within the cluster and an increase in the distribution of vibratory energy levels, while an increase in background indicates an increased multiple-time scattering of light in collapsing nanoaggregates.

The changes were more pronounced in the IPS-coupled systems. At 2% IPS, the relative contrast of the primary mode decreased on day 12, and broad collective vibration components appeared in the range of 400–900 cm^{-1}, indicating that theC_{60}–C60 interactions increased and clustering began. In 4% IPS, the process intensified, the primary mode expanded significantly and the maximum intensity decreased. At 8% IPS, the spectral deformation reached its maximum on day 12: the peaks widened, the intensity of the low-frequency modes increased, and the background level rose sharply; this indicates that the system approached the colloidal state and that large nanoaggregates were formed.

Note. Given that the frequency of ≈993 cm^{-1} is also close to the ring ("respiration") vibration of benzene, it is recommended to further compare the differences in contrast and width obtained from this substance with the specific modes of C_{60} (e.g., $A_g(2)$ ≈1470 cm^{-1} and H_g category) so that it will be possible to distinguish precisely the solvent contribution and the fullerene contribution.

3.6. Complex discussion of results and aggregation mechanism

A cross-comparison of the results of all methods shows that C_{60} aggregation is a stepwise process dependent on IPS proportion and time factor. In benzene, C_{60} molecules are surrounded by a stable solvation shell, present mainly in the form of small clusters of ≈17 nm according to YDS, a narrow and contrasting peak is observed in the Raman spectrum, and a monomer-specific peak of 391 nm is observed in the UV–Vis spectrum. With the addition of IPS, the effective dielectric properties of the medium change, the balance of solvent–molecule and molecule–molecule interactions is redistributed, π–π and dispersion (van der Waals) effects are intensified. As a result, 391 nm peak is lost, n and ρ decreases, the dominant size on YDS increases from 17 nm to ≈31 nm (4%), ≈80–120 nm (6%), and ≈150–220 nm (8%).

HSR (LONDON),
HOUGHTON STREET REVIEW JOURNAL
ISSN: 2058-5519|Impact factor-15.9
http://houghtonstreetreview.com/index.php/hsr

Time-based measurements complement this picture: in low IPS stakes (2–4%) there is compaction (n, ρ and Brix increase) and transition to a quasi-stable nanoaggregate state 4–8 days after initial clustering, while in higher stakes (6–8%) spatial destabilization, large aggregate formation, and polydispersion increase are manifested by day 12. The nonlinear variation of n, ρ and Brix over time indicates that aggregation is not a simple monotony, but rather a structural reorganization/aging mechanism. The summarized scheme is as follows: disperse monomer state → solved state → clustering → large nanoaggregates (→ coagulation and partial precipitation).

The proportion of "critical" IPS identified in the study (≈6%) was expressed differently in different properties of the system: optical density maximum in UV–Vis, plateau stabilization at n and ρ, predominance of aggregates of 80–120 nm in YDS. These changes corresponded to the intensive phase of aggregation, and long-term observations revealed the onset of destabilization (decrease in n, ρ and Brix on day 12) in this composition. These results confirm that the size of fullerene nanoaggregates in mixed solvents can be controlled through solvent composition.

4. CONCLUSION

1. An increase of 2 to 8% of the IPS fraction in the C60/benzene/IPS system reduces the refractive index of the solution from 1.4949 to 1.4851, the density from 0.8672 to 0.8564 g/cm3; this reflects a change in the balance of fullerene–solvent and fullerene–fullerene interactions and the formation of nanostructures.

2. In the UV–Vis spectra, the location of the peaks does not change much when IPS is added (the electronic structure C 60 is preserved), the monomer peak at 391 nm is lost, the optical density at 598.7 nm reaches a maximum at 6% IPS; The deviation from the Buger–Lambert–Ber law is associated with fullerene–fullerene interactions and the formation of aggregates.

3. The YDS method directly confirmed the aggregation: the dominant cluster size was ≈17 nm in benzene, IPS = ≈31 nm at 4%, ≈80–120 nm at 6%, ≈150–220 nm at 8%; Very large aggregates of 300–650 nm also occur at 8%, the system approaches the monodisperse to the polydisperse state and the coagulation stage.

4. At 1–12 day observations, the n, ρ, Brix, and Raman spectra showed a gradual progression of aggregation: compaction and quasi-stable nanoaggregates are formed at low IPS stakes (2–4%), while at high stakes (6–8%) spatial destabilization, large aggregate formation, and increased microheterogenicity are observed.

5. The obtained results serve as an experimental basis for the control of control of fullerene nanoaggregates, their optical properties and for the design of stable fullerene systems for nanocomposite films, photosensitive materials, organic optoelectronics and sensor technologies.

REFERENCES

1. Kroto H.W., Heath J.R., O'Brien S.C., Curl R.F., Smalley R.E. C60: Buckminsterfullerene // Nature. – 1985. – Vol. 318. – P. 162–163. https://doi.org/10.1038/318162a0

HSR (LONDON),
HOUGHTON STREET REVIEW JOURNAL
ISSN: 2058-5519|Impact factor-15.9
http://houghtonstreetreview.com/index.php/hsr

2. Goodarzi S., Da Ros T., Conde J., Sefat F., Mozafari M. Fullerene: biomedical engineers get to revisit an old friend // Materials Today. – 2017. – Vol. 20. – P. 460–480. https://doi.org/10.1016/j.mattod.2017.03.017
3. Shetty N.P., Mishra A., Basu S., Aminabhavi T.M. Versatile fullerenes as sensor materials // Materials Today Chemistry. – 2021. – Vol. 20. – Art. 100454. https://doi.org/10.1016/j.mtchem.2021.100454
4. Segura J.L., Giacalone F., Gómez R., Martín N., Guldi D.M., Luo C., Swartz A., Riedel I., Chirvase D., Parisi J. et al. Design, synthesis and photoelectrical properties of [60]fullerene-based molecular materials // Materials Science and Engineering C. – 2005. – Vol. 25. – P. 835–842. https://doi.org/10.1016/j.msec.2005.06.017
5. Deguchi S., Alargova R.G., Tsujii K. Stable dispersions of fullerenes, C_{60} and C70, in water. Preparation and characterization // Langmuir. – 2001. – Vol. 17. – P. 6013–6017. https://doi.org/10.1021/la010651o
6. Alargova R.G., Deguchi S., Tsujii K. Stable colloidal dispersions of fullerenes in polar organic solvents // J. Am. Chem. Soc. – 2001. – Vol. 123. – P. 10460–10467. https://doi.org/10.1021/ja010202a
7. Aich N., Boateng L.K., Sabaraya I.V., Das D., Flora J.R.V., Saleh N.B. Aggregation kinetics of higher-order fullerene clusters in aquatic systems // Environ. Sci. Technol. – 2016. – Vol. 50. – P. 3562–3571. https://doi.org/10.1021/acs.est.5b05447
8. Mchedlov-Petrossyan N.O., Marfunin M.O., Kriklya N.N. Colloid chemistry of fullerene solutions: aggregation and coagulation // Liquids. – 2024. – Vol. 4(1). – P. 32–72. https://doi.org/10.3390/liquids4010002
9. Marcus Y., Smith A.L., Korobov M.V., Mirakyan A.L., Avramenko N.V., Stukalin E.B. Solubility of C_{60} fullerene // J. Phys. Chem. B. – 2001. – Vol. 105. – P. 2499–2506. https://doi.org/10.1021/jp0023720
10. Hansen C.M., Smith A.L. Using Hansen solubility parameters to correlate solubility of C60 fullerene in organic solvents and in polymers // Carbon. – 2004. – Vol. 42. – P. 1591–1597. https://doi.org/10.1016/j.carbon.2004.02.011
11. Saraswati T.E., Setiawan U.H., Ihsan M.R., Isnaeni I., Herbani Y. The study of the optical properties of C_{60} fullerene in different organic solvents // Open Chemistry. – 2019. – Vol. 17(1). – P. 1198–1212. https://doi.org/10.1515/chem-2019-0117
12. Wei L., Yao J., Fu H. Solvent-assisted self-assembly of fullerene into single-crystal ultrathin microribbons and their highly sensitive UV–Vis photodetectors // ACS Nano. – 2013. – Vol. 7. – P. 7573–7582. https://doi.org/10.1021/nn402889h
13. Makhmanov U.K., Kokhkharov A.M., Bakhramov S.A., Erts D. The formation of self-assembled structures of C_{60} in solution and in the volume of an evaporating drop of a colloidal solution // Lithuanian Journal of Physics. – 2020. – Vol. 60, No. 3. – P. 194–204. https://doi.org/10.3952/physics.v60i3.4306

HSR (LONDON),
HOUGHTON STREET REVIEW JOURNAL
ISSN: 2058-5519|Impact factor-15.9
http://houghtonstreetreview.com/index.php/hsr

14. Makhmanov U.K. Refractive and electrophysical properties of dispersed solutions of fullerene C_{60} in binary solvents // Journal of Engineering Physics and Thermophysics. – 2022. – Vol. 95(2). – P. 527–532. https://doi.org/10.1007/s10891-022-02508-9
15. Makhmanov U.K., Kokhkharov A.M., Bakhramov S.A., Esanov S.A., Erts D. Self-assembly of C_{60} fullerene molecules in the hexane–xylene solvent system // Fullerenes, Nanotubes and Carbon Nanostructures. – 2022. – Vol. 30(1). – P. 80–84. https://doi.org/10.1080/1536383X.2021.1992390
16. Makhmanov U.K., Ismailova O., Kokhkharov A., Zakhidov E., Bakhramov S. Features of self-aggregation of C_{60} molecules in toluene prepared by different methods // Physics Letters A. – 2016. – Vol. 380 (24). – P. 2081–2084. https://doi.org/10.1016/j.physleta.2016.04.030
17. Makhmanov U.K., Esanov S.A., Aslonov B.A., Sun M., Chuliev T.A., Yusupov D.B., Bakhramov S.A., Kokhkharov A.M. // Fullerenes, Nanotubes and Carbon Nanostructures. – 2024. – Vol. 32(9). – P. 1–6. https://doi.org/10.1080/1536383X.2024.2374811
18. Makhmanov U.K., Kokhkharov A.M., Aslonov B.A., Esanov Sh.A., Bekmurodov Z., Musurmonov K.N., Shukurov A.X., Chuliyev T.A. Behavior of fullerene C_{60} in xylene/dimethylformamide binary solvents // Uzbek Journal of Physics. – 2024. – Vol. 26(1). – P. 1–5. https://doi.org/10.52304/.v26i1.490
19. Chen K.L., Elimelech M. Relating colloidal stability of fullerene (C60) nanoparticles to nanoparticle charge and electrokinetic properties // Environ. Sci. Technol. – 2009. – Vol. 43(19). – P. 7270–7276. https://doi.org/10.1021/es900185p
20. Brant J., Lecoanet H., Wiesner M.R. Aggregation and deposition characteristics of fullerene nanoparticles in aqueous systems. – 2005. – Vol. 7. – P. 545–553. https://doi.org/10.1007/s11051-005-4884-8